



Effect of Zr addition on the mechanical properties of Nb–Si based alloys

M. Sankar^{a,b,*}, G. Phanikumar^b, V.V. Satya Prasad^a



^a Defence Metallurgical Research Laboratory, Kanchanbagh, Hyderabad, 50005, India

^b Department of Metallurgical and Materials Engineering, Indian Institute of Technology Madras, Chennai, 600036, India

ARTICLE INFO

Keywords:

Electron microscopy
Hardness
Intermetallics
Phase transformation
Plasticity

ABSTRACT

In the present study, the effect of Zr addition on the mechanical properties of arc melted hypoeutectic Nb–16 at. %Si alloy has been investigated. The alloys were characterized by scanning electron microscopy (SEM), electron back scattered diffraction (EBSD), hardness test, nanoindentation test, compression test and three point bend test. The desirable phase α –Nb₅Si₃ phase could be obtained in alloys containing 4 at. % or more Zr. Nanoindentation results showed that the elastic modulus of Nb_{ss} phase is not significantly influenced by Zr additions whereas elastic modulus of Nb₃Si and α –Nb₅Si₃ phases are considerably improved by Zr additions. The strength, plasticity and room temperature fracture toughness of the alloys are significantly increased with Zr addition. The maximum compressive strength of 2160 ± 80 MPa, plastic strain of 2.6 ± 0.2% and fracture toughness of 14.3 ± 0.3 MPam^{1/2} are achieved in alloy with 4 at.% Zr.

1. Introduction

Nickel based superalloys in the form of single crystal turbine blades have been extensively used in the hottest section of the gas turbine engines. The skin temperature of these superalloys has already reached their maximum temperature limit of 1150 °C which is 85% of melting temperature of the alloys [1,2]. Scope for increasing the operating temperature beyond 1150 °C is limited because of localised melting that could occur due to the microsegregation of alloying elements. However, there is a desire among the modern gas turbine engine manufacturers to enhance the operating temperature of turbine blades above 1150 °C. This rise in temperature can ultimately lead to an increase in thermodynamic efficiency and reduce CO₂ emission during operation of the gas turbine engines. Therefore, there is an urgent need for development of new high temperature materials which can survive beyond the usage of current generation nickel base superalloys.

Alloys based on Nb–Si system are promising for next generation gas turbine blade applications owing to their high melting temperature (> 1750 °C), relatively low density (6.6–7.2 g/cc), high temperature strength and creep resistance. However, their low room temperature fracture toughness and poor oxidation resistance at high temperature are the major obstacles to use them for high temperature applications [3–5]. Nb–Si based alloys are also called as in-situ composites consisting of Nb silicide (Nb₃Si/Nb₅Si₃) matrix and Nb solid solution (Nb_{ss}) reinforcement. In these composites, Nb_{ss} phase provides room temperature fracture toughness and niobium silicide phase offers high

temperature strength and creep resistance. In binary Nb–Si based alloys, the high temperature phase Nb₃Si gets retained at room temperature because of its sluggish decomposition [6,7]. Moreover it has been reported that the Nb–Si alloys with Nb₃Si phase exhibits inferior creep resistance [8,9]. Hence, the alloy should be subjected to high temperature and long duration heat treatment for conversion of Nb₃Si phase in to Nb_{ss} and α –Nb₅Si₃ phases through a eutectoid transformation. However, the transformation takes more than 100 h to complete even at the nose of TTT diagram [6]. It is desirable to target improvement in mechanical properties of Nb–Si based alloys containing Nb_{ss} and α –Nb₅Si₃ phases in their microstructures because these are equilibrium phases and offer stability during service at high temperature [10].

The potential applications of Nb–Si based alloys at high temperature cannot be realized without achieving a balanced combination of properties of good high temperature strength and oxidation resistance combined with adequate room temperature fracture toughness. Different approaches such as alloying other elements and advanced fabrication techniques (powder metallurgy, directional solidification, etc.) have been attempted to improve the properties in the Nb–Si based alloys [11–16]. A brief summary of alloying of Nb–Si is reported in an earlier work [17]. There are limited studies on the effect of Zr addition on the microstructure and mechanical properties of binary Nb–Si alloys. The results on the microstructure evolution of Nb–16 at. % Si alloys [17] are encouraging. In this study, we present a detailed mechanical characterization of these alloys.

* Corresponding author. Defence Metallurgical Research Laboratory, Kanchanbagh, Hyderabad, 50005, India. Fax: +91 04024342316.
E-mail address: msankar_iitm@yahoo.co.in (M. Sankar).

2. Experimental work

Four alloy pancakes with nominal compositions of Nb–16Si%(A2), Nb–16Si%–2Zr%(AZ2), Nb–16Si%–4Zr% (AZ4) and Nb–16Si%–6Zr%(AZ6) were used in the present study. The alloys were prepared by non-consumable electrode arc melting in a water cooled copper mould under an argon atmosphere. The details of the alloy preparation methods have been elaborated in an earlier work [17]. All the compositions of the alloys are mentioned in at. % throughout the text. The phases and microstructures of the alloys were investigated by X-ray diffraction (XRD), scanning electron microscope (SEM) and electron back scattered diffraction (EBSD). Microhardness of the constituent phases was measured by UHL VMHT[®] make microhardness tester. Nanoindentation test was carried out to measure the modulus of elasticity of the constituent phases with a strain rate of $5 \times 10^{-2} \text{ s}^{-1}$. Berkovich[™] diamond indenter tip was used during nanoindentation test. The indenter tip was calibrated with fused silica samples before starting the test. The slope of the unloading portion of the load – displacement curve was used to determine the elastic modulus. The samples were cut from the alloy pancakes by electro discharge machining (EDM) for microstructure characterization, three point bend test and compression test. The same metallographic samples were used for both microhardness and nanoindentation study. Compression tests were conducted at room temperature using the Instron[®] 5500 R universal testing machine at a strain rate of $1 \times 10^{-3} \text{ s}^{-1}$. The dimensions of the compression test samples were 5 mm in diameter and 7.5 mm in height. The fracture toughness of the alloys was measured by conducting three point bend tests using an Instron[®] 5500 R universal testing machine with a cross head speed of 0.1 mm/min and a span of 20 mm. Single edge notched bending (SENB) specimens with 30 mm length, 6 mm width and 3 mm thickness were used for carrying out three point bend test. A 0.1 mm notch was introduced in the width side to $a/w = 0.5$, where ‘a’ is notch length and ‘w’ is width of the specimen. The fracture toughness measurements (K_Q) were performed according to ASTM E399 [18]. The K_Q values are calculated using the following equation.

$$K_Q = \frac{P_Q S}{Bw^{3/2}} f\left(\frac{a}{w}\right)$$

Where

P_Q is the maximum force during bend specimen testing,
 B is the specimen thickness,
 S is the length of span,
 w is the width of specimen,
 a is the length of notch.

The fracture surfaces of three point bend tested samples were analyzed by SEM using secondary electron imaging.

3. Results and discussion

The phases observed in Nb–16Si alloys containing different concentration of Zr are shown in Table 1. The typical XRD patterns of these alloys were presented in our earlier report [17]. It can be seen that from Table 1 that Zr free alloy (A2) exhibited Nb_{ss} and Nb₃Si phases. The alloy AZ2 exhibited Nb_{ss}, Nb₃Si and γ –Nb₅Si₃ phases. In contrast, the

Table 1
Phases observed in Nb–16%Si alloy containing different concentration of Zr by XRD.

Sl.No	Alloy composition (at. %)	Phases observed
1	Nb–16%Si (A2)	Nb _{ss} and Nb ₃ Si
2	Nb–16%Si–2%Zr (AZ2)	Nb _{ss} , Nb ₃ Si and γ –Nb ₅ Si ₃
3	Nb–16%Si–4%Zr (AZ4)	Nb _{ss} and α –Nb ₅ Si ₃
4	Nb–16%Si–6%Zr (AZ6)	Nb _{ss} , α –Nb ₅ Si ₃ and γ –Nb ₅ Si ₃

alloys AZ4 and AZ6 revealed Nb_{ss} and α –Nb₅Si₃ phases. Further, the alloy AZ6 also showed an additional phase namely γ –Nb₅Si₃. The SEM micrographs of Nb–16Si alloys containing various concentration of Zr are shown in Fig. 1. It can be seen that the binary alloy (A2) and alloy with 2%Zr (AZ2) primarily composed of Nb_{ss} and Nb₃Si phases. Conversely, the alloys AZ4 and AZ6 mainly composed of Nb_{ss} and α –Nb₅Si₃ phases. However, an additional phase is seen in the interdendritic region of alloys AZ2 and AZ6. The EBSD phase mappings of the alloys are shown in Fig. 2. The alloys A2 and AZ2 mainly exhibit Nb_{ss} and Nb₃Si phases while the main phases in alloys AZ4 and AZ6 are Nb_{ss} and α –Nb₅Si₃. EBSD results confirm that the additional phase seen in the interdendritic region of alloys AZ2 and AZ6 is γ –Nb₅Si₃ (hP16Mn₅Si₃– type, D₈). Thus, it follows that addition of 2%Zr has only a minor influence on the modification of microstructure in the as cast condition. In contrast, higher Zr addition has a significant influence on the modification of microstructures in alloys AZ4 and AZ6. The formation of interdendritic γ –Nb₅Si₃ phase in alloys AZ2 and AZ6 may be attributed to the enrichment of Si and Zr elements in the last stage of liquid to solidify during solidification of alloys. This is in agreement with the results of Tian et al. [19] on Nb–16Si–24Ti containing Zr. The enrichment of the liquid alloy with Si and Zr may also be attributed to their very low solid solubility in Nb. The Nb₃Si phase is totally absent in alloys AZ4 and AZ6. Instead, the alloys exhibited an equilibrium phases comprising of Nb_{ss} and α –Nb₅Si₃ in the as cast (i.e. arc melted) condition. The γ –Nb₅Si₃ phase is a product of eutectoid decomposition of Nb₃Si phase (Nb₃Si → Nb_{ss} + α –Nb₅Si₃). In the present study, it may be inferred that the eutectoid decomposition of Nb₃Si phase proceeds to completion when Zr concentration is above 2%. Probable mechanisms for the formation of Nb_{ss} and α –Nb₅Si₃ phases in Nb–Si alloy containing Zr in the as cast condition were explored earlier [17]. The formation of equilibrium microstructures consisting of Nb_{ss} and α –Nb₅Si₃ phases in the as cast condition is highly desirable for Nb–Si based alloys because it eliminates the need for high temperature and long duration vacuum heat treatment practice which is generally adopted for these alloys for conversion of Nb₃Si phase in to Nb_{ss} and α –Nb₅Si₃ phases.

The microhardness of the major phases present in the alloys as a function of Zr concentration is shown in Fig. 3. The hardness of Nb_{ss} phase in binary alloy (A2) is 454 ± 11 VHN and increases marginally to 487 ± 17 VHN with the addition of 2%Zr (AZ2). Thereafter, the hardness values decreases to 469 ± 11 VHN and 441 ± 8 VHN respectively in alloys AZ4 and AZ6 with further increase in the concentration of Zr above 2%. The hardness of Nb₃Si phase in Zr free alloy (A2) is 924 ± 14 VHN; it increases to 1225 ± 23 VHN in AZ2 alloy. This increase in hardness is attributed to the solid solution strengthening of Nb₃Si phase by Zr. As shown in Fig. 3, the hardness of α –Nb₅Si₃ phase is 1467 ± 35 VHN in alloy AZ4. The hardness value of α –Nb₅Si₃ phase decreases to 1274 ± 30 VHN in alloy AZ6. This shows that a large difference in hardness values of α –Nb₅Si₃ phase is noticed between alloys AZ4 and AZ6 despite the fact that the silicide phase exists in a same crystal structure in both the alloys. The reduction in hardness of α –Nb₅Si₃ phase in alloy AZ6 may be attributed to the solid solution softening of α –Nb₅Si₃ phase by Zr. This indicates that that the alloying element Zr plays a significant role to alter the hardness of Nb–Si alloys. A minor fraction of hexagonal γ –Nb₅Si₃ phase was observed in alloys AZ2 and AZ6. However, the small size of the γ –Nb₅Si₃ phase precluded reliable measurement of hardness.

Nanoindentation experiments were conducted on Nb_{ss} and silicide phases of sufficiently large size. Load was chosen to ensure indentation is significantly smaller than size of the phase to avoid effect of interface. The loads of 30 mN and 15 mN were used for indentation of Nb₃Si and Nb_{ss} phases respectively in alloys A2 and AZ2. While the loads of 20 mN and 15 mN were used for indentation of α –Nb₅Si₃ and Nb_{ss} phases respectively in alloys AZ4 and AZ6. The typical load versus displacement curves of the nanoindentation test performed on Nb–Si alloy containing different Zr concentration are shown in Fig. 4. It can be seen

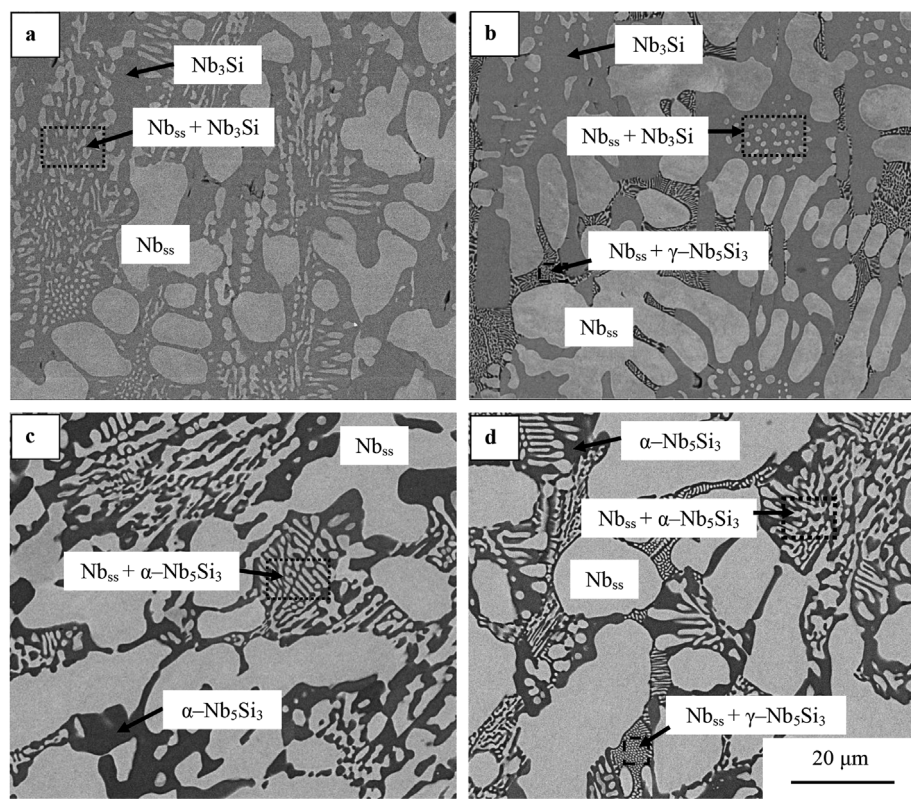


Fig. 1. SEM BSE micrographs of Nb–16Si alloy containing Zr: (a) 0 Zr, (b) 2Zr, (c) 4Zr and (d) 6Zr.

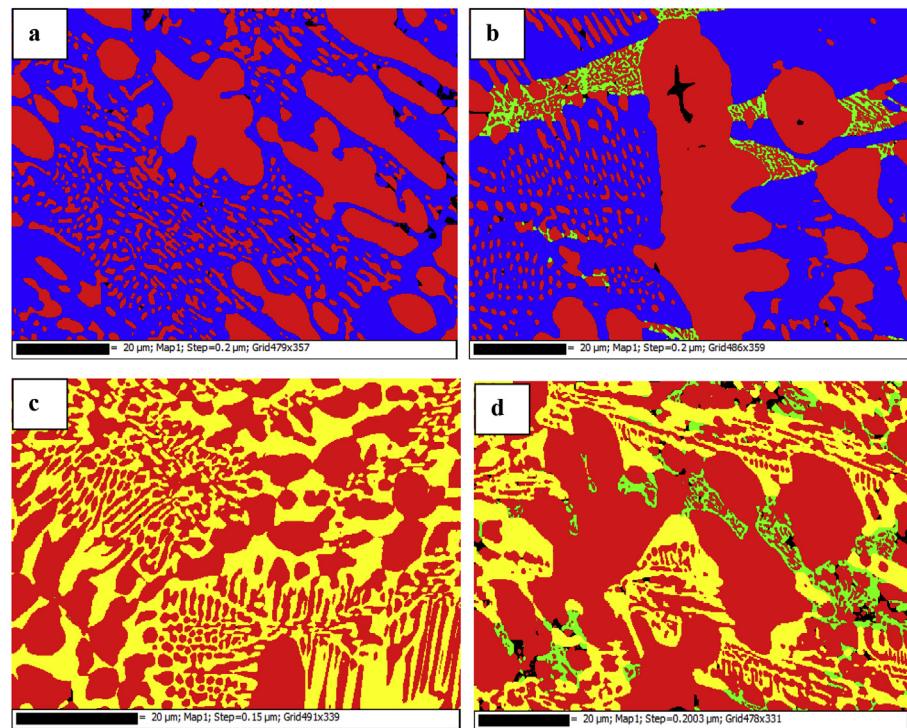


Fig. 2. EBSD phase mapping showing phases of Nb–16 Si alloy containing Zr: (a) A2, (b) AZ2, (c) AZ4 and (d) AZ6. In this figure red colour represents Nb_{ss}, blue colour represent Nb₃Si, green colour represents γ -Nb₅Si₃ and yellow colour represents α -Nb₅Si₃. (For interpretation of the references to colour in this figure legend, the reader is referred to the Web version of this article.)

that the depth of indentation of Nb_{ss} phase decreases with 2% Zr as compared to Zr free alloy for the same indentation load. On the other hand, no significant change in indentation depth is observed in Nb₃Si phase. Poisson ratio values of 0.2 for silicide phase and 0.35 for Nb_{ss} phase were used to calculate elastic modulus using nanoindentation test [20]. The measured elastic modulus of Nb_{ss}, Nb₃Si and Nb₅Si₃ phases as

a function of different Zr concentration are presented in Fig. 5. The elastic modulus of Nb_{ss} phase is not significantly influenced by Zr addition. In contrast, a large difference in elastic modulus of Nb₃Si and α -Nb₅Si₃ phases was noticed in Nb–Si alloy containing Zr. The elastic modulus of Nb₃Si phase is 252 ± 13 GPa in Zr free alloy (A2) while the elastic modulus of the Nb₃Si phase in 2%Zr added alloy (AZ2) is

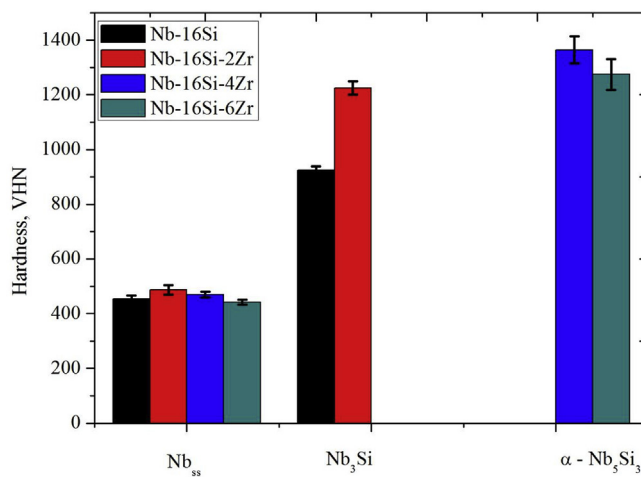


Fig. 3. Bar chart showing microhardness of phases present in Nb-16Si containing Zr.

273 ± 9 GPa. It indicates that the bonding of Nb_3Si phase gets changed and becomes stronger when 2% Zr is added to Nb-Si alloy as compared to Zr free alloy. The elastic modulus value obtained for $\alpha - \text{Nb}_5\text{Si}_3$ phase is 355 ± 13 GPa in alloy AZ4. This value is significantly higher than that of the elastic modulus value reported for monolithic Nb_5Si_3 (327 GPa) [20]. Further, it is obvious from Fig. 5 that the elastic modulus of $\alpha - \text{Nb}_5\text{Si}_3$ phase decreases to 316 ± 4 GPa when Zr concentration exceeds 4%. However, the elastic modulus of $\alpha - \text{Nb}_5\text{Si}_3$

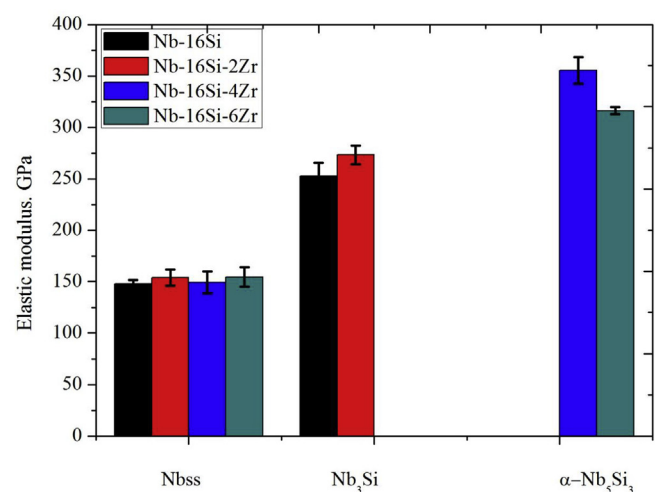


Fig. 5. Bar chart showing elastic modulus of constituent phases present in Nb-16Si containing Zr.

phase in alloy AZ6 is comparable to that of the elastic modulus reported in the literature. The different elastic modulus values of $\alpha - \text{Nb}_5\text{Si}_3$ phase in the Nb-Si alloys containing varying Zr content can be attributed to the dissolution of Zr in the phase possibly due to weakening the bonding in the intermetallic phase by Zr.

The room temperature compressive strength and plasticity of the alloys as measured by compression test are shown in Fig. 6. It can be

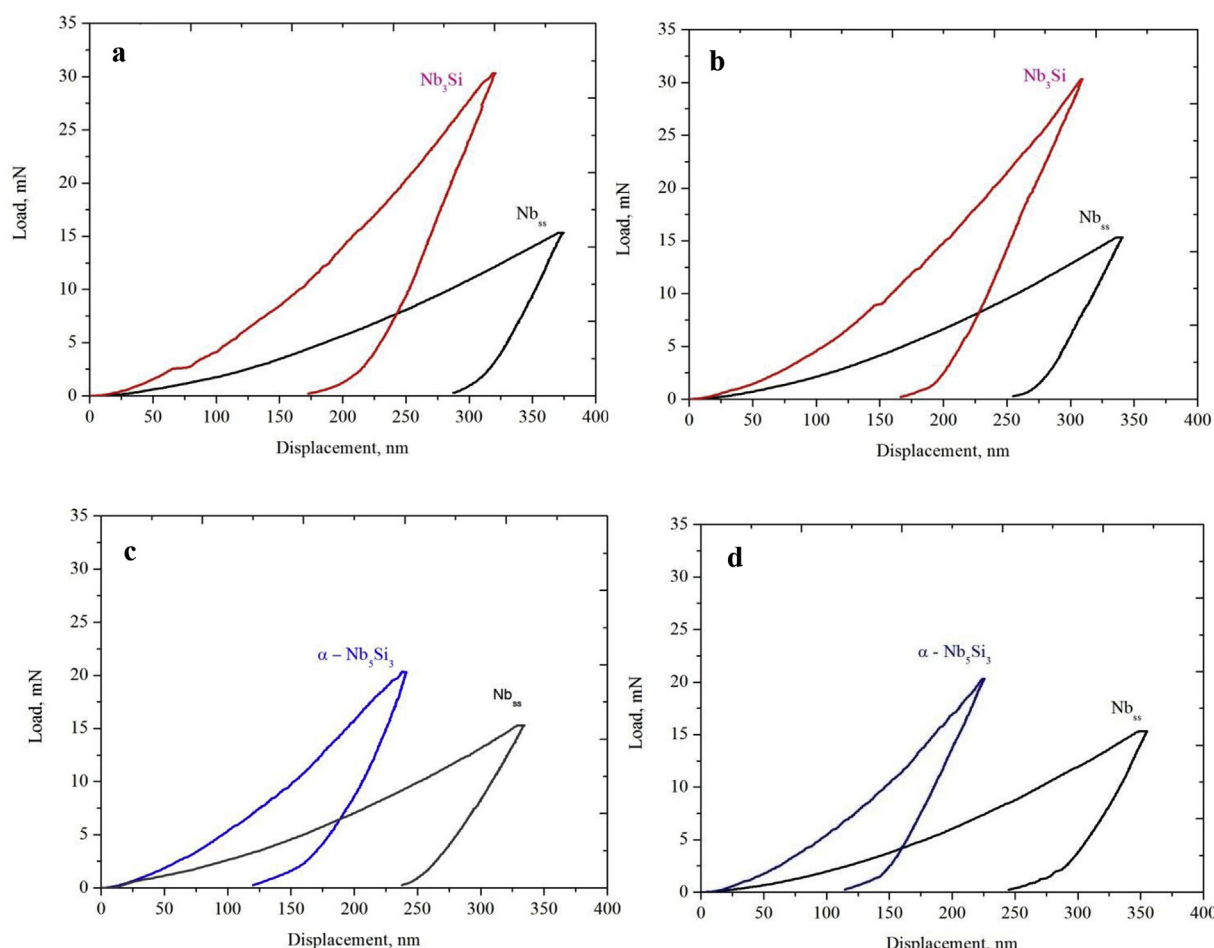


Fig. 4. Shows the typical load – displacement curves obtained from nanoindentation test of Nb-16Si alloy containing Zr: (a) 0Zr, (b) 2Zr, (c) 4Zr and (d) 6Zr.

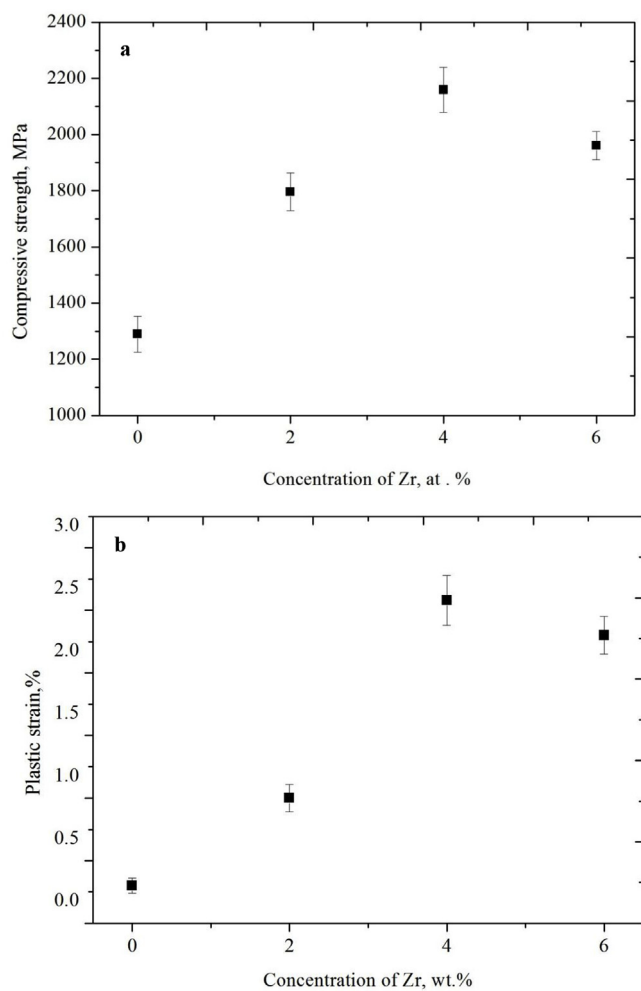


Fig. 6. Plots showing room temperature mechanical properties of Nb–16 alloy containing Zr: (a) Compressive strength and (b) Plastic strain.

Table 2
Volume fraction of phase present in the alloys.

Nominal alloy composition (at %)	Volume fraction (%)			
	Nb _{ss}	Nb ₃ Si	γ-Nb ₅ Si ₃	α-Nb ₅ Si ₃
Nb–16Si (A2)	48.66 ± 0.61	51.34 ± 0.56	–	–
Nb–16Si–2Zr (AZ2)	44.06 ± 1.59	50.47 ± 1.63	5.47 ± 0.07	–
Nb–16Si–4Zr (AZ4)	59.25 ± 0.51	–	–	40.75 ± 0.54
Nb–16Si–6Zr (AZ6)	63.18 ± 1.22	–	6.18 ± 0.2	30.64 ± 0.92

seen from Fig. 6a that the compressive strength of binary Nb–16Si alloy (A2) is 1289 ± 64 MPa. The compressive strength increases to 1795 ± 67 MPa when 2% Zr is added to Nb–16Si alloy (AZ2). The alloy AZ4 exhibited a maximum compressive strength of 2159 ± 79 MPa. Further, the compressive strength of alloy decreases to 1960 ± 50 MPa when concentration of Zr increased to 6% (AZ6). It can be seen from Fig. 6b that the plastic strain of alloys increased with increase in concentration of Zr up to 4%. Thereafter, plastic strain of the alloys decreased with further increase in Zr concentration to 6%. This trend is akin to the behavior of compression strength of Nb–16Si alloy containing different concentration of Zr. The increase in compressive strength and plastic strain of alloys with Zr addition is related to the volume fraction and morphology of Nb_{ss} and Nb₃Si/Nb₅Si₃ phases. The

volume fractions of various phases present in the alloys are shown in Table 2 [17]. The decrease in volume fraction of Nb_{ss} phase from $48.66 \pm 0.61\%$ to $44.06 \pm 1.59\%$ along with solid solution strengthening of Nb₃Si phase (volume fraction: $50.47 \pm 1.63\%$) by Zr is responsible for improvement in strength of alloy AZ2 as compared to Zr free alloy (A2). The maximum compressive strength and plastic strain achieved in alloy AZ4 is related to the change in microstructure and morphology of the phases. It has been reported that the Nb–Si based alloys with lamellar microstructure consisting of Nb_{ss} and α–Nb₅Si₃ exhibits better combination of mechanical properties [21]. Therefore, in the present study the higher compressive strength achieved in alloy AZ4 is in agreement with results reported by Sekido et al. [21]. Besides, the solid solution of α–Nb₅Si₃ phase by Zr is also responsible for increase in compressive strength of alloy AZ4 as Zr atoms are expected to substitute for Nb site of α–Nb₅Si₃ phase. Beyond the maximum values of compressive strength and plastic strain of alloy AZ4, the decrease in both compressive strength and plastic strain of alloy AZ6 may be attributed to the presence of γ–Nb₅Si₃ phase with volume fraction of approximately 6%. The γ–Nb₅Si₃ phase has been reported to be hard and brittle [22]. Further, the increase in volume fraction of Nb_{ss} phase from $59.25 \pm 0.51\%$ (AZ4) to $63.18 \pm 1.22\%$ (AZ6) and decrease in volume fraction of α–Nb₅Si₃ phase from $40.75 \pm 0.54\%$ (AZ4) to $30.64 \pm 0.92\%$ (AZ6) is also partially responsible for drop in compressive strength of alloy AZ6 as compared to alloy AZ4.

A reasonable fracture toughness at room temperature is one of the important properties of materials used for high temperature structural applications. The Nb–Si based alloys are basically in-situ composites consisting of the ductile Nb_{ss} phase and the hard niobium silicide phases. The Nb_{ss} phase provides room temperature fracture toughness while the Nb₅Si₃ phase imparts high temperature strength. The primary toughening mechanisms of these alloys are crack bridging, crack arrest and crack deflection of Nb_{ss} phase. In addition, the fracture toughness of Nb–Si based alloys is also related to the volume fraction and morphology of Nb_{ss} and Nb₃Si/Nb₅Si₃ phases. The room temperature fracture toughness of the alloys as determined by the three point bend test is shown in Fig. 7. The reported values are an average of three test results. It can be seen that the fracture toughness of the alloys increased with increase in concentration of Zr, reached maximum in alloy AZ4 and then it decreased with further increase in Zr concentration to 6% (AZ6).

Table 3 lists the fracture toughness values of some of the binary, ternary and multicomponent Nb–Si based alloys processed under different processing conditions for comparison. It can be seen from Table 3 that the fracture toughness of the Nb–Si based alloys is sensitive to the

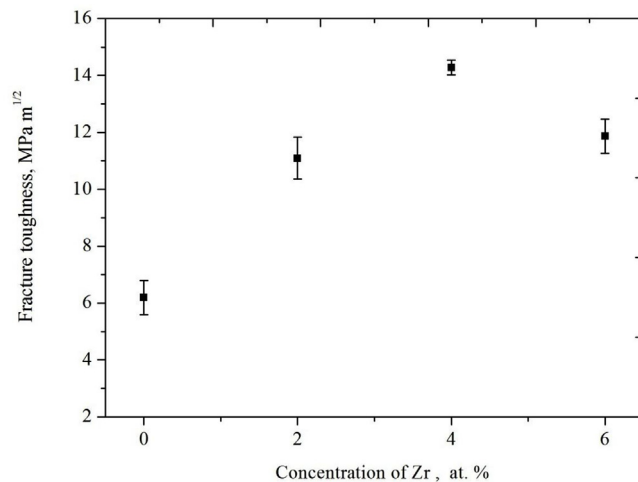


Fig. 7. Plot showing the room temperature fracture toughness of Nb–16 Si alloy containing Zr. 50 μm.

Table 3

Comparison of fracture toughness values of Nb–Si based alloys with different compositions.

Alloy composition (at.%)	Processing method	Testing method	Fracture toughness (MPam ^{1/2})	References
Nb ₅ Si ₃	HP + HT@1500 °C	Three point bend test	3	[21]
Nb–10Si	AM	Three point bend test	9.2	[24]
	AM + HT@1500 °C/100 h		9.7	
	AM + E		16.44	
	AM + E + HT@1500 °C/100 h		20.66	
Nb–16Si	AM		5.4	
	AM + HT@1500 °C/100 h		7.35	
	AM + E + HT at 1500 °C/100 h		12.5	[25]
Nb–16Si–1Hf	AM	Three point bend test	7.3	[26]
Nb–16Si–3Hf			7.5	
Nb–16Si–7Hf			8.5	
Nb–18.7Si	AM	Three point bend test	8.4	[27]
Nb–18.7Si–10Ti	AM		11.8	
Nb–17.5Si–10Ti	DS		9.8	
Nb–17.5Si–10Ti	DS + HT		16.0	
Nb–16Si–5Mo	AM	Three point bend test	8.5	[28]
Nb–16Si–15Mo			10.2	
Nb–16Si–2Fe	AM	Three point bend test	9.37	[29]
	AM + HT@ 1350 °C/100 h		10.19	
Nb–16Si–4Fe	AM		9.03	
	AM + HT@ 1350 °C/100 h		9.63	
Nb–16Si–6Fe	AM		9.66	
	AM + HT@ 1350 °C/100 h		9.51	
Nb–17Si–10Mo – 0.1Ga	DS	Four point bend test using	9.3	[30]
Nb–17Si–10Mo – 0.1Ga	DS + HT@1300 °C/100 h		12.0	
Nb–17Si–10Mo –1Ga	DS		6.6	
Nb–17Si–10Mo –1Ga	DS + HT@1300 °C/100 h		10.5	
Nb–22Ti–15Si–5Cr–3Hf–3Al	AM	Three point bend test	11.94	[31]
Nb–22Ti–15Si–5Cr–3Hf–3Al–2Zr			12.89	
Nb–22Ti–15Si–5Cr–3Hf–3Al–4Zr			13.73	
Nb–22Ti–15Si–5Cr–3Hf–3Al–8Zr			15.01	
Nb–15Si–24Ti–4Cr–2Al–2Hf	AM + DS + HT@1450 °C	Three point bend test	9.87	[32]
Nb–15Si–24Ti–4Cr–2Al–2Hf–1V			12.98	
Nb–16Si–20Ti–3Al–2Hf–6Cr– 4V	AM	Three point bend test	9.9	[33]
Nb–16Si–20Ti–3Al–2Hf–6Cr– 2V			11.13	
Nb–16Si–20Ti–3Al–2Hf–3Cr– 4V			14	
Nb–16Si–20Ti–3Al–2Hf–3Cr– 2V			14.72	

AM- Arc melted, HT-Heat treated, DS-Directionally solidified, E-Extruded, IM-Induction melted, HP-Hot pressed.

chemical composition and the processing technologies. It is also clear from Table 3 that the fracture toughness of binary alloy is a function of silicon content. The room temperature fracture toughness of monolithic Nb₅Si₃ phase is 3 MPam^{1/2} [23]. For the as cast binary Nb–Si alloys, the fracture toughness values are 9.2 MPam^{1/2} and 5.4 MPam^{1/2} for the arc melted Nb–10Si and Nb–16Si alloys respectively [24,25]. The fracture toughness value of these alloys are increased to 9.7 (for Nb–10Si alloy) and 7.54 MPam^{1/2} (for Nb–16Si alloy) even after high temperature and long duration vacuum heat treatment (i.e. 1500 °C for 100 h). Table 3 also reveals that the fracture toughness of Nb–Si alloy was significantly improved by thermomechanical processing. For example, the Nb–10Si alloy exhibits higher fracture toughness values of 16.44 MPam^{1/2} after extrusion and 20.66 MPam^{1/2} after extrusion and heat treatment as against the fracture toughness of 9.2 MPam^{1/2} in the as cast condition [24,25]. Besides, it is clear that directional solidification and alloying with other elements also considerably enhances the fracture toughness of Nb–Si based alloys [26–33]. In the present study, it is found that the addition of Zr resulted in a significant improvement in the values of room temperature fracture toughness of Nb–Si alloys (Fig. 7).

The fracture toughness value of Zr free alloy (A2) is comparable to that of literature data reported for binary Nb–16Si alloy. The fracture toughness values obtained for alloy AZ4 is 14.3 ± 0.3 MPam^{1/2}. This value is significantly high compared to other alloy composition investigated in the present study and promising. The volume fraction of Nb_{ss} phase plays a major role for the improvement in the fracture toughness of Nb–Si based alloys. In the present work, the volume fraction of Nb_{ss} phase increases with increase in concentration of Zr except for alloy with 2%Zr (AZ2). The increase in volume fraction of

Nb_{ss} phase resists the crack propagation more effectively and increases the fracture toughness of Nb–Si based alloys through the mechanisms of crack bridging, crack arrest and crack deflection.

The alloys A2 and AZ2 exhibit the eutectic Nb_{ss} phase in form of rods in a continuous matrix of Nb₃Si phase. Hence, fracture toughness is limited in these alloys A2 and AZ2. However, the higher fracture toughness achieved in alloy AZ2 as compared to alloy A2 is attributed to the solid solution strengthening of Nb_{ss} and Nb₃Si phases by Zr. It has been reported that the Nb–Si based alloys with a lamellar microstructure composed of Nb_{ss} and α–Nb₅Si₃ phases shows higher fracture toughness [21,27]. In the present study, the alloys AZ4 and AZ6 exhibit lamellar morphology of Nb_{ss} and α–Nb₅Si₃ phases. Thus, both the alloys (AZ4 and AZ6) are expected to have higher fracture toughness. However, the fracture toughness of alloy AZ6 is less (10.8 ± 0.6 MPam^{1/2}) as compared to the fracture toughness of alloy AZ4 (14.3 ± 0.3 MPam^{1/2}) in spite of the fact that the alloy AZ6 displays lamellar microstructure. The decrease in fracture toughness of alloy AZ6 is similar to the behavior of decrease in compressive strength and plastic strain of alloy AZ6. This is associated with microstructure of alloys AZ4 and AZ6. It can be inferred from the EBSD phase mapping depicted in Fig. 2 that the alloy AZ4 composed of only Nb_{ss} and α–Nb₅Si₃ phases (i.e free from the γ–Nb₅Si₃ phase) while the alloy AZ6 has approximately 6% volume fraction of γ–Nb₅Si₃ phase along with Nb_{ss} and α–Nb₅Si₃ phases. The γ–Nb₅Si₃ phase has been reported to have an adverse effect on the fracture toughness of Nb–Si based alloys [11].

The fracture toughness of Nb–Si based alloys in presence of hexagonal γ–Nb₅Si₃ phase has been investigated by many authors [32,34]. It has been reported that γ–Nb₅Si₃ phase generally forms in Nb–Si

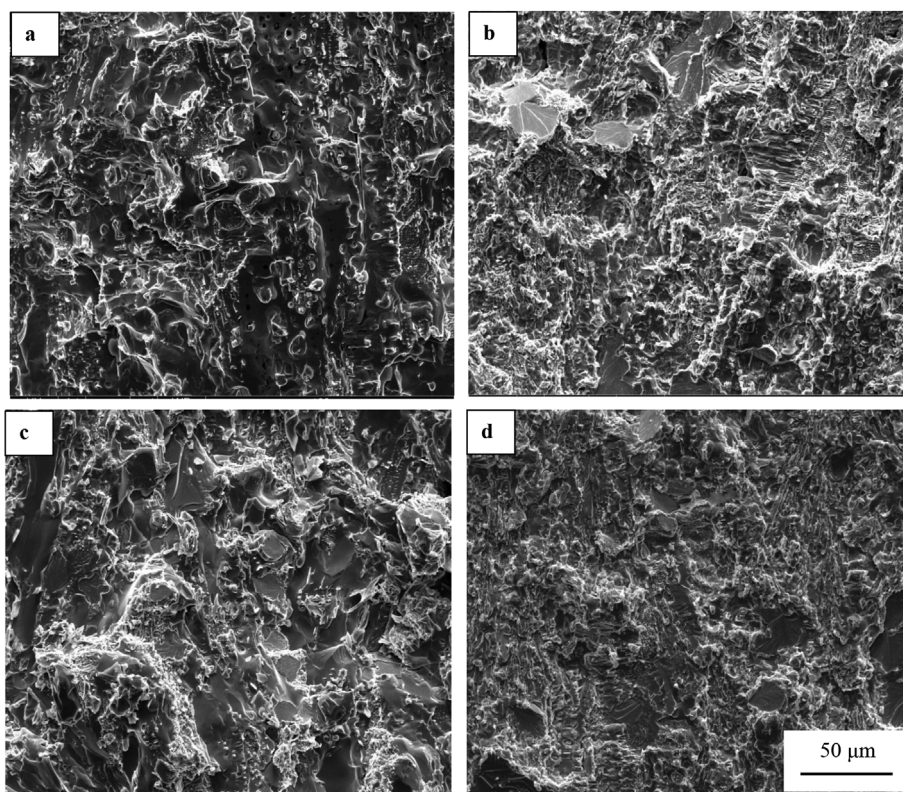


Fig. 8. SEM fractographs showing fracture surfaces of three point bend tested samples of Nb–16 Si alloy containing Zr: (a) 0Zr, (b) 2Zr, (c) 4Zr and (d) 6Zr.

alloys containing higher concentration of Ti and Hf. The γ –Nb₅Si₃ phase is more brittle as compared to α –Nb₅Si₃ phase in Nb–Si based alloys. Therefore, in the present study, it is confirmed that the reduction in fracture toughness values in alloy AZ6 as compared to alloy AZ4 is solely attributed to the presence of γ –Nb₅Si₃ phase. Alloy composition alone, however, is not sufficient to ensure high fracture toughness. It should be noted that the size of the Nb_{ss} phase also plays a significant role to ensure higher fracture toughness of Nb–Si based alloys. Sekido et al. [27] and Kim et al. [28] have shown that the resistance to crack propagation can be very effective when Nb_{ss} plate is thick. In the present study, the thickness eutectoid Nb_{ss} plate is more in alloy AZ4 as compared to alloy AZ6. Therefore, the higher fracture toughness values achieved in alloy AZ4 is well in agreement with the literature [27,28].

Secondary electron imaging of the fracture surfaces of the three point bend tested samples (Fig. 8) shows that primary Nb_{ss} and Nb₃Si phases failed in a brittle cleavage mode with large facets in alloys A2 and AZ2. Whereas Nb_{ss} phase revealed both the cleavage fracture with river pattern and a few ductile tearing ridges in alloys AZ4 and AZ6. The fracture mode of Nb₅Si₃ phase is almost same in both alloys AZ4 and AZ6 with brittle cleavage pattern. However, the amount of the plastic tearing ridges in alloy AZ4 is much larger than the ones noticed in alloy AZ6. The more amounts of the tearing ridges in Zr added alloy particularly in alloy AZ4 is contributing to enhance the fracture toughness at room temperature, since the tearing ridge is a manifestation of plastic fracture mode.

4. Conclusions

In the present study, the microstructure and mechanical properties of Nb–16Si alloy containing different concentrations of Zr were systematically investigated. The conclusions drawn are as follows.

1. The Nb_{ss} and Nb₃Si are main phases in alloys A2 (Nb–16Si) and AZ2 (Nb–16Si–2Zr) while Nb_{ss} and α –Nb₅Si₃ are main phases in alloys

AZ4 (Nb–16Si–4Zr) and AZ6 (Nb–16Si–6Zr). Small amounts of γ –Nb₅Si₃ phase is found in alloys AZ2 and AZ6.

2. Zr is an effective solid solution strengthener of Nb₃Si and Nb₅Si₃phases.
3. The modulus of elasticity of silicide phases is significantly increased with Zr addition. The highest value of modulus of elasticity is obtained for alloy containing 4% Zr.
4. The strength, plasticity and fracture toughness of the alloy increase with increase in concentration of Zr up to 4% Zr. Thereafter, they decrease with increase in concentration of Zr to 6% due to the formation of γ –Nb₅Si₃ phase.

Acknowledgement

The authors are grateful to Defence Research and Development Organisation, Ministry of Defence, New Delhi for the financial support in carrying out this research work. The authors wish to thank Dr. Vikas Kumar, Director, DMRL for his keen interest and encouragement. The authors also would like to thank officers and staff of electroslag remelting group and electron microscopy group for giving technical support to carry out this work.

References

- [1] C. Rogers, Reed, the Superalloys: Fundamentals and Applications, Cambridge University Press, New York, 2006.
- [2] B.P. Bewlay, M.R. Jackson, M.F.X. Gigliotti, R.L. Fleischer, J.H. Westbrook (Eds.), Intermetallic Compounds–Principles and Practice, vol. 3, John Wiley, New York, NY, 2001, pp. 541–560.
- [3] B.P. Bewlay, M.R. Jackson, J.C. Zhao, Ultrahigh–temperature Nb–silicide-based composites, *MRS Bull.* 28 (9) (2003) 636–646.
- [4] B.P. Bewlay, M.R. Jackson, J.C. Zhao, P.R. Subramanian, A review of very high temperature Nb silicide –based composites, *Metall. Mater. Trans.* 34 (10) (2003) 2043–2052.
- [5] P.R. Subramanian, M.G. Mendiratta, D.M. Dimiduk, M.A. Stucke, Advanced intermetallic alloys–beyond gamma titanium aluminides, *Mater. Sci. Eng., A* 239–240 (1997) 1–13.
- [6] M.G. Mendiratta, D.M. Dimiduk, Phase relations and transformation kinetics in the

- high Nb region of the Nb–Si system, *Scripta Metall.* 25 (1) (1991) 237–242.
- [7] B. Cockeram, H.A. Lipsitt, R. Srinivasan, I. Weiss, Phase relationships in Nb-18.7 a/o Si In-situ composite, *Scripta Metall. Mater.* 25 (1991) 2109–2114.
- [8] K.S. Chan, Modelling creep behaviour of niobium silicide in-situ composites, *Mater. Sci. Eng., A* 337 (2002) 59–66.
- [9] B.P. Bewley, S.D. Sitzman, L.N. Brewer, M.R. Jackson, Analyses of eutectoid phase transformations in Nb–silicide in situ composites, *Microsc. Microanal.* 10 (2004) 470–480.
- [10] M.E. Schlesinger, H. Okamoto, A.B. Gokhale, The Nb–Si (Niobium–Silicon) system, *J. Phase Equilibria* 14 (1993) 502–509.
- [11] K.S. Chan, Alloying effects on fracture mechanisms in Nb-based intermetallic in-situ composites, *Mater. Sci. Eng., A* 329–331 (2002) 513–522.
- [12] L. Bendersky, F.S. Biancaniello, W.J. Boettinger, J.H. Perepezko, Microstructural characterization of rapidly solidified Nb–Si alloys, *Mater. Sci. Eng.* 89 (1987) 151–159.
- [13] B.P. Bewley, M.R. Jackson, W.J. Reeder, H.A. Lipsitt, Microstructures and properties of DS in-situ composites of Nb–Si–Ti alloys, *Mater. Res. Soc. Symp. Proc.* 364 (1995) 943–948.
- [14] Z. Li, M. Peng, Microstructure and mechanical properties of Nb-based in situ composites from Nb–Si–Ti ternary system, *Acta Mater.* 55 (2007) 6573–6585.
- [15] N. Sekido, Y. Kimura, S. Miura, Y. Mishima, Microstructure development of unidirectionally solidified (Nb)/Nb₅Si₃ eutectic alloys, *Mater. Sci. Eng., A* 444 (2007) 51–57.
- [16] Y. Guo, L. Jia, S. Sun, B. Kong, J. Liu, H. Zhang, Rapid fabrication of Nb–Si based alloy by selective laser melting: microstructure, hardness and initial oxidation behavior, *Mater. Des.* 109 (2016) 37–46.
- [17] M. Sankar, G. Phanikumar, Vaijinder Singh, V.V. Satya Prasad, Effect of Zr additions on microstructure evolution and phase formation of Nb–Si based ultrahigh temperature alloys, *Intermetallics* 101 (2018) 123–132.
- [18] ASTM E399-12 International, Standard Test Method for Linear-Elastic Plane-Strain Fracture Toughness of KIC Metallic Materials, ASTM International, West Conshohocken (PA), 2012.
- [19] X. Tian, J.T. Guo, L.Y. Sheng, G.M. Cheng, L.Z. Zhou, L.L. He, H.Q. Ye, Microstructure and mechanical properties of cast Nb–Ti–Si–Zr alloys, *Intermetallics* 16 (2008) 807–812.
- [20] J.H. Kim, T. Tabaru, H. Hirai, A. Kitahara, S. Hanada, Mechanical properties of Nb–18Si–5Mo–5Hf–2C in-situ composite prepared by arc casting method, *Mat. OR Trans.* 43 (9) (2002) 2201–2204.
- [21] N. Sekido, Y. Kimura, F.G. Wei, S. Miura, Y. Mishima, Effect of lamellar spacing on the mechanical properties of (Nb)/(Nb,Ti)₅Si₃ two-phase Alloys, *J. Jpn. Inst. Metals* 64 (11) (2000) 1056–1061.
- [22] K.S. Chan, Alloying effects on the fracture toughness of Nb-based silicides and laves phases, *Mater. Sci. Eng., A* 409 (1) (2005) 257–269.
- [23] R.K. Nekkanti, D.M. Dimiduk, Ductile-phase toughening in niobium–niobium silicide powder processed composite, *Mater. Res. Soc. Symp. Proc.* 194 (1990) 175–182.
- [24] M.G. Mendiratta, D.M. Dimiduk, Strength and toughness of a Nb/Nb₅Si₃ composite, *Metall. Trans. A* 24 (1993) 501–504.
- [25] M.G. Mendiratta, J.J. Lewandowski, D.M. Dimiduk, Strength and ductile phase toughening in the two phase Nb/Nb₅Si₃ alloys, *Metall. Trans. A* 22 (1991) 1573–1583.
- [26] Y.X. Tian, J.T. Guo, L.Z. Zhou, G.M. Cheng, H.Q. Ye, Microstructure and room temperature fracture toughness of cast Nb_{ss}/silicides composites alloyed with Hf, *Mater. Lett.* 62 (2008) 2657–2660.
- [27] N. Sekido, Y. Kimura, S. Miura, F.G. Wei, Y. Mishima, Fracture toughness and high temperature strength of unidirectionally solidified Nb–Si binary and Nb–Ti–Si ternary alloys, *J. Alloy compd.* 425 (2006) 223–229.
- [28] W.Y. Kim, H. Tanaka, A. Kasama, S. Hanada, Microstructure and room temperature fracture toughness of Nb_{ss}/Nb₅Si₃ in situ composites, *Intermetallics* 9 (2001) 827–834.
- [29] J.R. Zhou, J.B. Sha, Microstructural evolution and mechanical properties of an Nb–16Si in-situ composite with Fe additions prepared by arc-melting, *Intermetallics* 34 (2013) 1–9.
- [30] Y. Li, C. Ma, H. Zhang, S. Miura, Mechanical properties of directionally solidified Nb–Mo–Si-based alloys with aligned Nb_{ss}/Nb₅Si₃ lamellar structure, *Mater. Sci. Eng., A* 528 (2011) 5772–5777.
- [31] Y. Qiao, X. Guo, Y. Zeng, Study of the effects of Zr addition on the microstructure and properties of Nb–Ti–Si based ultrahigh temperature alloys, *Intermetallics* 88 (2017) 19–27.
- [32] Y. Guo, L. Jia, B. Kong, H. Zhang, H. Zhang, Simultaneous improvement in fracture toughness and oxidation resistance of Nb–Si based alloys by vanadium addition, *Mater. Sci. Eng., A* 701 (2017) 149–157.
- [33] Y. Kang, S. Qu, J. Song, Q. Huang, Y. Han, Microstructure and mechanical properties of Nb–Ti–Si–Al–Hf–xCr–yV multi-element in situ composite, *Mater. Sci. Eng., A* 534 (2012) 323–328.
- [34] S. Zhang, X. Guo, Effects of Cr and Hf additions on the microstructure and properties of Nb silicide based ultrahigh temperature alloys, *Mater. Sci. Eng., A* 638 (2015) 121–131.